# Determining Mixing Rates from Concurrent Temperature and Velocity Measurements

CYNTHIA E. BLUTEAU[a]

*School of Civil, Environmental and Mining Engineering, University of Western Australia, Perth, and UWA Oceans Institute, Crawley, Western Australia, Australia*

ROLF G. LUECK

*Rockland Scientific International, Inc., Victoria, British Columbia, Canada*

GREGORY N. IVEY AND NICOLE L. JONES

*School of Civil, Environmental and Mining Engineering, University of Western Australia, Perth, and UWA Oceans Institute, Crawley, Western Australia, Australia*

JEFFREY W. BOOK AND ANA E. RICE

*Oceanography Division, U.S. Naval Research Laboratory, Stennis Space Center, Mississippi*

(Manuscript received 22 December 2016, in final form 24 June 2017)

ABSTRACT

Ocean mixing has historically been estimated using Osborn's model by measuring the rate of dissipation of turbulent kinetic energy $\epsilon$ and the background density stratification $N$ while assuming a value of the flux Richardson number $\mathrm{Ri}_f$. A constant $\mathrm{Ri}_f = 0.17$ is typically assumed, despite mounting field, laboratory, and modeling evidence that $\mathrm{Ri}_f$ varies. This challenge can be overcome by estimating the turbulent diffusivity of heat $K_T$ using the Osborn–Cox model. This model, however, requires measuring the rate of dissipation of thermal variance $\chi$, which has historically been challenging, particularly in energetic flows because the high wavenumbers of the temperature gradient spectra are unresolved with current technology. To overcome this difficulty, a method is described that determines $\chi$ by spectral fitting to the inertial-convective (IC) subrange of the temperature gradient spectra. While this concept has been exploited for moored time series, particularly near the bottom boundary, it has yet to be adapted to vertical microstructure profilers such as gliders, and autonomous and ship-based vertical profilers from which there are the most measurements. By using the IC subrange, $\chi$, and hence $K_T$, can be estimated even in very energetic events—precisely the conditions requiring more field observations. During less energetic periods, the temperature gradient spectra can also be integrated to obtain $\chi$. By combining these two techniques, microstrucure profiles at a field site known for its very energetic internal waves are analyzed. This study demonstrates that the spectral fitting approach resolves intense mixing events with $K_T \gtrsim 10^{-2}\ \mathrm{m^2\ s^{-1}}$. By equating the Osborn and Osborn–Cox models, indirect estimates for $\mathrm{Ri}_f$ can also be obtained.

## 1. Introduction

Turbulent mixing controls the distribution of contaminants, nutrients, temperature, and small organisms in the ocean. For example, the vertical flux of nutrients across the pycnocline can control the input of nutrients to the euphotic zone, thereby governing ocean productivity (Gargett 1997). Prescription of the global ocean circulation and vertical heat transport depends critically on the diapycnal mixing (Wunsch and Ferrari 2004; De Lavergne et al. 2016). Circulation models rely on turbulence closure schemes to parameterize subgrid-scale mixing, and these parameterizations are derived from idealized engineering flows or from controlled experiments at length scales and turbulence intensities that are very different from those observed in the ocean

[a] Additional affiliation: Institut des Sciences de la Mer, Université du Québec à Rimouski, Rimouski, Quebec, Canada.

*Corresponding author*: Cynthia E. Bluteau, cynthia.bluteau@uwa.edu.au

DOI: 10.1175/JTECH-D-16-0250.1

(e.g., Mellor and Yamada 1982; Ivey et al. 2008; Salehipour et al. 2016). Thus, field observations of turbulent mixing remain essential to assessing and developing these models and to understanding the connections between large-scale physical processes and small-scale mixing.

Historically, the vast majority of turbulence measurements in the ocean have been obtained from vertically free-falling microstructure profilers (Lueck et al. 2002). Typically, these measurements are used to compute the rate of turbulent kinetic energy dissipation $\epsilon$ and, in turn, the eddy diffusivity for density $K_\rho$ using the model:

$$K_\rho = \left(\frac{\mathrm{Ri}_f}{1-\mathrm{Ri}_f}\right)\frac{\epsilon}{N^2}, \tag{1}$$

where $\mathrm{Ri}_f$ is the flux Richardson number and $N$ is the background buoyancy frequency (Osborn 1980). This relationship assumes a balance between shear production, buoyancy flux, and dissipation, and it requires an independent estimate of $\mathrm{Ri}_f$ (see Ivey et al. 2008). For example, Waterhouse et al. (2014) collated 5200 individual microstructure profiles collected at diverse sites over 30 years, and then assumed a constant value of $\mathrm{Ri}_f = 0.17$ in all measurements to estimate $K_\rho$ from (1). However, laboratory experiments (e.g., Rohr et al. 1988; Ivey and Nokes 1989; Strang and Fernando 2001; Rehmann and Koseff 2004), direct numerical simulations (DNS; e.g., Peltier and Caulfield 2003; Shih et al. 2005; Salehipour et al. 2015), and recent field observations (e.g., Davis and Monismith 2011; Dunckley et al. 2012; Bluteau et al. 2013; Walter et al. 2014; Holleman et al. 2016) all show that $\mathrm{Ri}_f$ varies.

Ongoing work attempts to describe the variability of $\mathrm{Ri}_f$ in terms of other dimensionless parameters, such as the gradient Richardson number $\mathrm{Ri} = N^2/S^2$ and the buoyancy Reynolds number $\mathrm{Re}_b = \epsilon/\nu N^2 = (L_O/\eta)^{4/3}$ (e.g., Mater and Venayagamoorthy 2014; Salehipour et al. 2016). Here $S$ is the mean shear, $\nu$ is the molecular kinematic viscosity, $L_O$ is the Ozmidov length scale (an estimate of the large-scale overturns), and $\eta$ is the Kolmogorov length scale. Despite these efforts the exact $\mathrm{Ri}_f$ value to use when estimating $K_\rho$ with (1), for any particular measurement of $\epsilon$, remains uncertain.

One way to circumvent the difficulty of specifying $\mathrm{Ri}_f$ is to estimate turbulent mixing from a method first suggested by Osborn and Cox (1972) by using both the velocity and fast-response temperature sensors that most microstructure profilers carry. Assuming a balance between the production of thermal variance by the vertical flux of heat acting against the background gradient of temperature $\overline{u_3'T'}\partial\overline{T}/\partial x_3$ and its dissipation by molecular diffusion $\chi$, the vertical diffusivity of heat $K_T$ is

$$K_T = \frac{1}{2}\frac{\chi}{\left(\frac{\partial\overline{T}}{\partial x_3}\right)^2}. \tag{2}$$

Here the background temperature gradient is along the $x_3$ (vertical) direction, $T$ is the temperature, and the overbar denotes a temporal average. By equating the Osborn model [(1)] to the Osborn–Cox model [(2)], an indirect measure of $\mathrm{Ri}_f$ can also be obtained (Oakey 1982):

$$\frac{\mathrm{Ri}_f}{1-\mathrm{Ri}_f} = \frac{N^2}{2\left(\frac{\partial\overline{T}}{\partial x_3}\right)^2}\frac{\chi}{\epsilon}. \tag{3}$$

Estimating turbulent mixing $K_T$ and $\mathrm{Ri}_f$ from (2) and (3) appears attractively simple, but in practice their application has been impeded by difficulties in obtaining reliable $\chi$ estimates. As discussed in detail below, $\chi$ has traditionally been estimated with information from the high-wavenumber end of the temperature gradient spectrum using two methods: either by integrating over these high wavenumbers (e.g., Sherman and Davis 1995; Ruddick et al. 2000) or by Batchelor spectrum fitting techniques at very high wavenumbers (e.g., Luketina and Imberger 2001; Merrifield et al. 2016). Both of these methods, however, are challenging because of the temperature sensor's poor response at high frequencies (e.g., Sommer et al. 2013, see section 2.1). Having the profiler move as slowly as 0.05–0.1 m $\mathrm{s}^{-1}$ in the vertical is one solution (Sherman and Davis 1995), but this restricts the number of profiles and hence the amount of sampling that can be achieved in deep oceanic water columns. The lack of sensor resolution is especially difficult for high-energy turbulent events—precisely those that need to be resolved and included if we are to measure the full range of turbulent processes in the ocean. The challenge is thus to develop practical ways to measure oceanic mixing rates from existing technology and data streams.

In this paper, we demonstrate how to use existing technology and/or datasets to determine $\chi$ from the more easily resolved inertial-convective subrange portion of the temperature gradient spectrum. Studies involving moored (time series) measurements have exploited the inertial-convective subrange (e.g., Bluteau et al. 2013; Holleman et al. 2016), but this practice has yet to be adapted to profiling microstructure turbulence measurements such as gliders, and autonomous and

ship-based profilers from which we have historically the most measurements. We describe the theoretical and practical aspects of the method, and demonstrate its application to observations from a site known for its energetic internal waves and hence high mixing rates. The presented techniques also provide an indirect measure for $\mathrm{Ri}_f$ [(3)], thus allowing the dependency of $\mathrm{Ri}_f$ on external parameters to be assessed. While the observations presented here are not exhaustive of all conditions prevailing in the ocean, they do demonstrate a way to quantify ocean mixing that is applicable to existing and future measurements.

## 2. Methods

### a. Theoretical background

#### 1) Traditional methods for determining $\chi$

The dissipation of thermal variance $\chi$ has traditionally been determined by integrating the temperature gradient spectrum to the high-wavenumber end of the viscous-diffusive subrange, thus requiring resolution of the highest wavenumbers of the temperature spectra. Term $\chi$ can be directly obtained from

$$\chi \equiv 2\kappa\overline{(\nabla T')^2}, \tag{4}$$

where $\kappa$ is the molecular diffusivity of heat. For isotropic turbulence, $\chi$ can be estimated from the turbulent temperature gradient measurements collected in one direction (Oakey 1982):

$$\chi_I = 6\kappa\overline{\left(\frac{\partial T'}{\partial x_3}\right)^2} = 6\kappa\int_0^\infty \Phi_{\partial T/\partial x_3}(k)dk \tag{5}$$

and is equivalent to integrating the one-sided temperature gradient spectral observations $\Phi_{\partial T/\partial x_3}$, which yields our integrated estimate $\chi_I$. The concept is simple, but its application is hampered by theoretical and practical limitations. An integrated $\chi$ estimate can be obtained only when both the viscous-convective and viscous-diffusive subranges are resolved. Resolving the entire viscous-diffusive subrange is, however, difficult, since the measured spectra must be substantially corrected (sometimes up to a factor of $\sim 10^3$) due to the poor response of temperature sensors at high frequencies (see Fig. 1). Attempts to characterize the frequency response of the most popular sensor, the FP07 thermistor, have led to ambiguous results with respect to both the time constant of the sensor response and whether the response is single or double poled (Goto et al. 2016; Sommer et al. 2013; Nash et al. 1999; Hill 1987; Vachon and Lueck 1984). These ambiguities result partly because these sensors are "handmade" and hence differ in their physical dimensions, but mainly because calibrating their frequency response is difficult and no commercial facility exists for this service.

Many have attempted to fit the lower wavenumbers of the viscous-diffusive subrange with a model of the temperature gradient spectrum (e.g., Batchelor 1959; Kraichnan 1968; Ruddick et al. 2000; Sanchez et al. 2011; Merrifield et al. 2016) in order to "resolve" the high wavenumbers in the viscous subrange (Fig. 1). However, the universality of the constants used in these models are debated, particularly the root-mean-square of the rate of strain that is undetermined to a factor of 2 (e.g., Luketina and Imberger 2001). More importantly though, the viscous-diffusive subrange moves to higher wavenumbers $k$ with increasing $\epsilon$ (Fig. 1), making it more difficult to resolve. For example, at typical profiling speeds of 0.6–1 m $\mathrm{s}^{-1}$, the thermistor's response correction is more than a factor of 10 at the peak of the viscous-diffusive subrange for $\epsilon \approx 10^{-8}$ W $\mathrm{kg}^{-1}$, thus rendering the integration or spectral fitting of the viscous subranges unreliable for determining $\chi$ in energetic environments.

#### 2) Inertial-convective subrange method for obtaining $\chi$

There are a number of advantages in using the inertial-convective subrange. Located at lower wavenumbers than the viscous-diffusive subrange, the inertial-convective subrange is more readily resolved with the FP07 thermistor. Even at the fast profiling speeds, typical of vertical profilers, there is no (or very little) frequency response correction required within the inertial-convective subrange (Fig. 1). The universality of the theoretical form in this subrange is also much less debated than that in the viscous subranges. This theoretical temperature gradient model spectrum in the inertial-convective subrange is given by (Tennekes and Lumley 1972)

$$\Psi_{\partial T/\partial x_i}(k) = C_T\chi\epsilon^{-1/3}k^{1/3}, \tag{6}$$

where $k$ is the wavenumber (rad $\mathrm{m}^{-1}$) and $C_T$ is the Obukhov–Corrsin universal constant. Sreenivasan (1996) compiled observations from diverse published sources that yielded $C_T$ between 0.3 and 0.5. From this analysis, he recommended $C_T = 0.4$ and so like others (e.g., Geyer et al. 2008; Holleman et al. 2016), we set $C_T = 0.4$ and note that the possible range for $C_T$ between 0.3 and 0.5 may bias $\chi_F$ by 25%.

To differentiate between the $\chi$ estimates obtained by integrating and fitting the temperature gradient

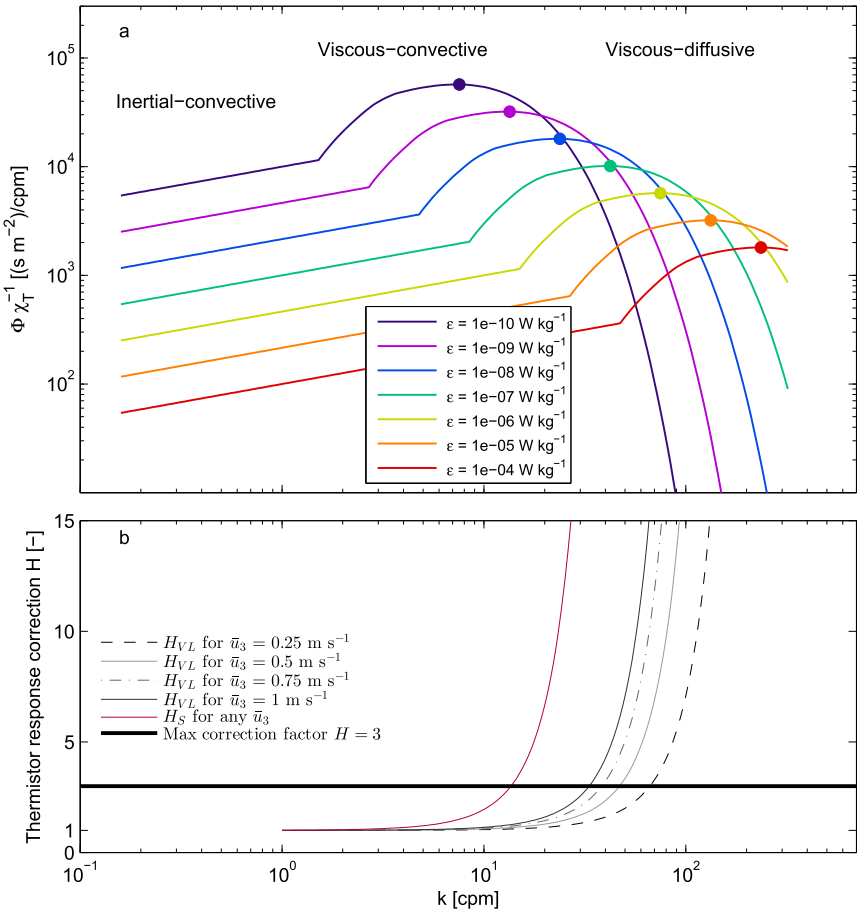


FIG. 1. (a) Kraichnan's model spectra for $\partial T/\partial x_3$ spectra for varying $\epsilon$ with the universal constant set to $q = 5.25$ (Bogucki et al. 2012). Also shown is the wavenumber where 25% of the variance (i.e., $\chi$) is resolved (circles). (b) The frequency response correction $H_{\mathrm{VL}}$ is dependent on the mean flow speed past the thermistor $\overline{u}_3$, while $H_S$ is the more aggressive frequency correction of Sommer et al. (2013) that is independent of $\overline{u}_3$.

spectrum, we use the subscripts $I$ and $F$, respectively, in the discussion below. Fitting the observed spectrum to obtain $\chi_F$ from (6) requires an a priori estimate of $\epsilon$ from the simultaneous velocity measurements. However, in practice, the value of $\chi_F$ is not strongly sensitive to the estimate of $\epsilon$ because of the $\epsilon^{1/3}$ dependence in (6). More importantly, determining $\chi_F$ from the inertial-convective subrange of the spectrum becomes easier in energetic environments because the smallest and largest wavenumbers become increasingly separated with increasing turbulence intensity and hence $\mathrm{Re}_b$. This, in turn, allows $\chi_F$ to be obtained for high $\epsilon$ from the inertial-convective subrange of temperature spectra located over similar $k$ as the inertial-subrange of velocity spectral observations.

Observationally, the inertial subrange of velocity measurements extends to $k\eta \approx 0.1$ (see Gargett et al. 1984). At this limit, the slope of the compensated shear spectrum deviates by 1% of its expected value, while about 15% of the variance of the shear spectrum is resolved (Nasmyth 1970; Oakey 1982; Wolk et al. 2006). With decreasing $\mathrm{Re}_b$, however, the lowest wavenumbers are increasingly impacted by the mean flow. The spectral properties in the vertical direction are more adversely affected by stratification than those in the longitudinal direction. Gargett et al. (1984), for example, observed an inertial subrange in the longitudinal velocity spectra until $\mathrm{Re}_b \lesssim 180$, while an inertial subrange in their vertical velocity spectra was lost for $\mathrm{Re}_b \lesssim 450$. The vertical temperature gradient spectra $\Phi_{\partial T/\partial x_3}$ are therefore considered unusable for estimating $\chi_F$ when $\mathrm{Re}_b \lesssim 450$; however, this threshold can be relaxed to $\mathrm{Re}_b \lesssim 180$ for moored measurements that yield horizontal temperature gradient spectra $\Phi_{\partial T/\partial x_1}$.

*b. Analysis procedures*

The frequency spectra obtained from $\Phi_{\partial T/\partial x_3}(f)$ are corrected for the thermistor's frequency response using a double-pole transfer function

$$H(f) = [1 + (2\pi\tau f)^2]^{-2} \tag{7}$$

with a time constant $\tau = \tau_o(\overline{u}_3/u_o)^{-1/2}$, where $\tau_o = 4.1 \times 10^{-3}$ s and $u_o = 1.0\,\mathrm{m\,s^{-1}}$ (Vachon and Lueck 1984). Other, more aggressive, relationships for the frequency response correction have been proposed (Hill 1987; Nash et al. 1999; Sommer et al. 2013) but, as shown in Fig. 1, the correction impacts only the highest $k$ of the inertial-convective subrange for large $\epsilon \gtrsim 10^{-5}\,\mathrm{W\,kg^{-1}}$. In our assessment below, we evaluate both the frequency response correction of Vachon and Lueck (1984), denoted as $H_{\mathrm{VL}}$, and the more aggressive frequency response correction proposed by Sommer et al. (2013), denoted as $H_S$, which is independent of the mean flow velocity $\overline{u}_3$, that is, $\tau = 1 \times 10^{-2}$ s. We then convert the corrected $\Phi_{\partial T/\partial x_3}(f)$ into wavenumber spectral observations $\Phi_{\partial T/\partial x_3}(k)$ using the mean vertical profiling speed $\overline{u}_3$ via Taylor's frozen turbulence hypothesis. These spectral observations can then be either fitted or integrated to obtain $\chi_F$ or $\chi_I$, respectively.

1) SPECTRAL FITTING PROCEDURES TO OBTAIN $\chi_F$

To derive $\chi_F$, we assume that $\epsilon$ has been determined from the inertial and/or viscous subranges of turbulent velocity or velocity gradient measurements (e.g., Bluteau et al. 2011b, 2016). The segment length from the profile used to compute the temperature gradient spectra must be sufficiently long to resolve the wavenumbers within the inertial-convective subrange, which moves to lower wavenumbers with decreasing $\epsilon$ (Fig. 1). For low $\epsilon \approx 10^{-9}\,\mathrm{W\,kg^{-1}}$, the chosen segment length and spectral averaging strategy must ensure that $k \approx 2\,\mathrm{rad\,m^{-1}}$ (0.3 cpm) is resolved to allow for enough spectral bandwidth to fit the inertial-convective subrange.

We use the maximum likelihood estimator (MLE) [e.g., Eq. (3) of Bluteau et al. 2016] to fit the inertial-convective subrange model [(6)] to the observed wavenumber spectral observations $\Phi_{\partial T/\partial x_3}(k)$. The MLE relies on an assumed statistical distribution for the observations. In this instance, the ratios $d[\Phi(k)/\Psi(k)]$ are $\chi^2_d$ distributed (Emery and Thomson 2001), with $d$ representing the number of degrees of freedom of the estimated spectra $\Phi_{\partial T/\partial x_3}(k)$. Within the inertial-convective subrange, given the larger number of spectral observations with increasing $k$, we rely mainly on the information from the higher and hence more isotropic wavenumbers $k$. The lower $k$, potentially more adversely impacted by the mean flow, are excluded by applying the mean absolute deviation (MAD) misfit criteria proposed by Ruddick et al. (2000),

$$\mathrm{MAD} = \left| \frac{1}{n} \sum_{i=1}^{n} \left[ \frac{\Phi(k_i)}{\Psi(k_i)} - \left\langle \frac{\Phi(k_i)}{\Psi(k_i)} \right\rangle \right] \right|, \tag{8}$$

to short subsets of the spectra approximately 0.5–0.7 of a decade long. Here, $n$ refers to the number of individual $i$ spectral observations $\Phi(k)$ used to fit the theoretical spectra $\Psi(k)$ in (6). If all subsets of the spectrum yielded a MAD $>2(2/d)^{1/2}$ (Ruddick et al. 2000), then the spectrum is completely discarded. Otherwise, the final wavenumber range used to obtain $\chi_F$ starts at the lowest wavenumber at which MAD$<2(2/d)^{1/2}$ and ends at either $k \lesssim 0.1\eta^{-1}$ or the wavenumber at which the frequency response correction exceeds 3, that is, $k \approx 40$ cpm for $\overline{u}_3 = 0.6\,\mathrm{m\,s^{-1}}$ in Fig. 1.

2) SPECTRAL INTEGRATION PROCEDURES TO OBTAIN $\chi_I$

Ideally, $\chi_I$ should be estimated via (5) when a significant portion of the temperature gradient variance within both the viscous-convective and viscous-diffusive subranges are resolved (see, e.g., Sherman and Davis 1995; Ruddick et al. 2000). With increasing $\epsilon$, these subranges move to higher wavenumbers and so we use the Batchelor wavenumber $k_B = [\epsilon/(\nu\kappa^2)]^{1/4}\,(\mathrm{rad\,m^{-1}})$ to identify the position of the viscous-diffusive subrange. An integrated $\chi_I$ estimate is deemed acceptable if the temperature gradient spectra can be integrated for up to $k < 0.3\,k_B$, for which almost half of the variance contributing to $\chi_I$ is resolved. The maximum wavenumber that can be integrated $k_{mI}$ depends on the acceptable correction factor of the thermistor's frequency response, but the noise-dominated wavenumbers must also be avoided. Here, we use a maximum factor correction of 3 for the frequency response, corresponding to $k \approx 30 - 50$ cpm for the correction factor of Vachon and Lueck (1984), and $k \approx 10$ cpm for the more aggressive correction of Sommer et al. (2013) (Fig. 1b). This maximum frequency correction factor thus restricts the integration method to $\epsilon \lesssim 5 \times 10^{-8}\,\mathrm{W\,kg^{-1}}$.

For low $\epsilon$ cases, a spectral rolloff is often observed prior to instrument noise dominating the spectral observations. To avoid the noise-dominated wavenumbers, we identify the local minima of the smoothed (band averaged) spectra between $0.2\,k_B$ and $k_B$. We set $k_{mI}$ to the global local minimum but, if none is found, $k_{mI}$ is set to $k_B$. The temperature gradient spectra $\Phi_{\partial T/\partial x_3}(k)$ is then integrated from the lowest spectral observation to

$k_{mI}$ [(5)]. The variance is then adjusted to account for the unresolved variance according to the proportion of variance that should be resolved as a function of $k/k_B$ using Kraichnan's model spectrum with the same universal constant $q_K$ recommended by Bogucki et al. (2012). This adjusted value represents $\chi_I$, which is retained as the $\chi$ estimate for the given segment if the flow is not energetic enough (i.e., low $\mathrm{Re}_b$) to use the fitted estimate $\chi_F$. For some intermediate energy segments, it is valid to estimate both $\chi_I$ and $\chi_F$, and the two can be compared.

## 3. Field measurements

The abovementioned methods for estimating $\chi$ and $\mathrm{Ri}_f$ were applied to observations from the Australian North West shelf, known for its ubiquitous and highly energetic internal waves (e.g., Holloway et al. 2001; Bluteau et al. 2011a). We applied the methods to 118 successful vertical turbulence profiles collected with a VMP-500 (Rockland Scientific Ltd.) over a 24-h period starting at 0700 UTC 10 April 2012. Each hour consisted of five successive VMP profiles that were collected over a period of 25 min. Sampling at 512 Hz, the VMP was equipped with two airfoil probes collecting the velocity gradients used to estimate $\epsilon$ from the methods described by Bluteau et al. (2016); 3D accelerometers were used to remove motion-induced contamination from the velocity gradient spectra (Goodman et al. 2006); and a pressure sensor was used to determine the instrument's profiling speed $\overline{u}_3$. Typical drop speeds were 0.5–0.8 m $\mathrm{s}^{-1}$. The majority of the returned $\epsilon$ estimates from these measurements ranged between $10^{-9}$ and $10^{-6}$ W $\mathrm{kg}^{-1}$ (Bluteau et al. 2016). In addition to the abovementioned sensors, the VMP was equipped with high-accuracy temperature and conductivity sensors (SBE-3F and SBE-4C from Sea-Bird Electronics) that sampled at 64 Hz to provide the mean background stratification $N$ and temperature gradients $\partial\overline{T}/\partial x_3$. A fast-response temperature sensor (FP07), sampling at 512 Hz, provided the measurements to estimate $\chi$.

The temperature gradient spectra were obtained from the FP07 measurements over the same segments used to determine $\epsilon$. Each of the 118 vertical profiles were split into segments of 2048 samples (4 s) that overlapped by 50%. The temperature gradient spectra were estimated by applying an FFT on 512 point-long (1 s) subsets with a 50% overlap. A Hanning window was applied to each subset in the time domain, which resulted in temperature gradient spectra with more than 21 degrees of freedom. For each segment, these spectra were used to obtain $\chi$ with either the integrated or fitted technique, and for some intermediate energy segments with both techniques. We determined mixing rates $K_T$ from (2) using these $\chi$ estimates and the background temperature gradient $\partial\overline{T}/\partial x_3$ determined from the temperature profiles collected by SBE-3F aboard the VMP. To obtain the background temperature gradient, each individual temperature profile was smoothed with a fourth-order Butterworth low-pass filter with a cutoff period of 1.5 s (i.e., ~0.8–1.2 m) and then depth averaged over the segment depth range used to estimate $\epsilon$ and $\chi$.

## 4. Results and assessment

The observed temperature gradient spectra, for a range of $\epsilon$ covering almost four decades, are compared in Fig. 2 against the Kraichnan model (Kraichnan 1968; Bogucki et al. 2012) and the inertial-convective subrange models [(6)]. We corrected the spectral observations for the FP07's frequency response using two separate relationships, but neither can recover the viscous-diffusive subrange (Fig. 2). With the gentle frequency correction $H_{\mathrm{VL}}$ of Vachon and Lueck (1984), the spectral observations in the viscous-diffusive subrange show less energy than predicted by the Kraichnan spectrum (e.g., Figs. 2a,b), while the frequency response proposed by Sommer et al. (2013) overcorrects the spectra (i.e., $H_S > 3$) within this subrange. The viscous-diffusive subrange is unresolved (overcorrected) with either frequency correction in the high $\epsilon$ examples (Figs. 2e,f).

Similar conclusions can be reached by comparing the model cumulative integrated spectra to the observed spectra obtained after applying both the $H_S$ and $H_{\mathrm{VL}}$ frequency corrections. Integrating the observed spectra corrected with $H_{\mathrm{VL}}$ underpredicted $\chi$ (Figs. 2c,d), while the corrected spectra with $H_S$ followed the integrated model spectrum more closely. For the highest $\epsilon = 10^{-5}$ W $\mathrm{kg}^{-1}$ example shown, the model deviated strongly from the observations because both the viscous-convective and viscous-diffusive subranges were located in the noise-dominated $k$ range (Fig. 2f). Integrating over these $k$ thus overestimated $\chi$ (Fig. 2h). In this high $\epsilon$ example, avoiding the noise-dominated $k$ by integrating up to $k \approx 70$ cpm would not solve the problem, since less than 10% of the variance was resolved at this $k$, while the frequency response correction was almost two orders of magnitude (Fig. 1). The observations were, however, in good agreement with the inertial-convective subrange model and could thus be fitted with (6) to determine $\chi_F$.

Integrating the spectra to obtain $\chi$ was thus confined to periods of relatively weaker turbulence (i.e., low $\epsilon$), while fitting the spectra was generally confined to periods of more energetic turbulence (i.e., high $\mathrm{Re}_b$).

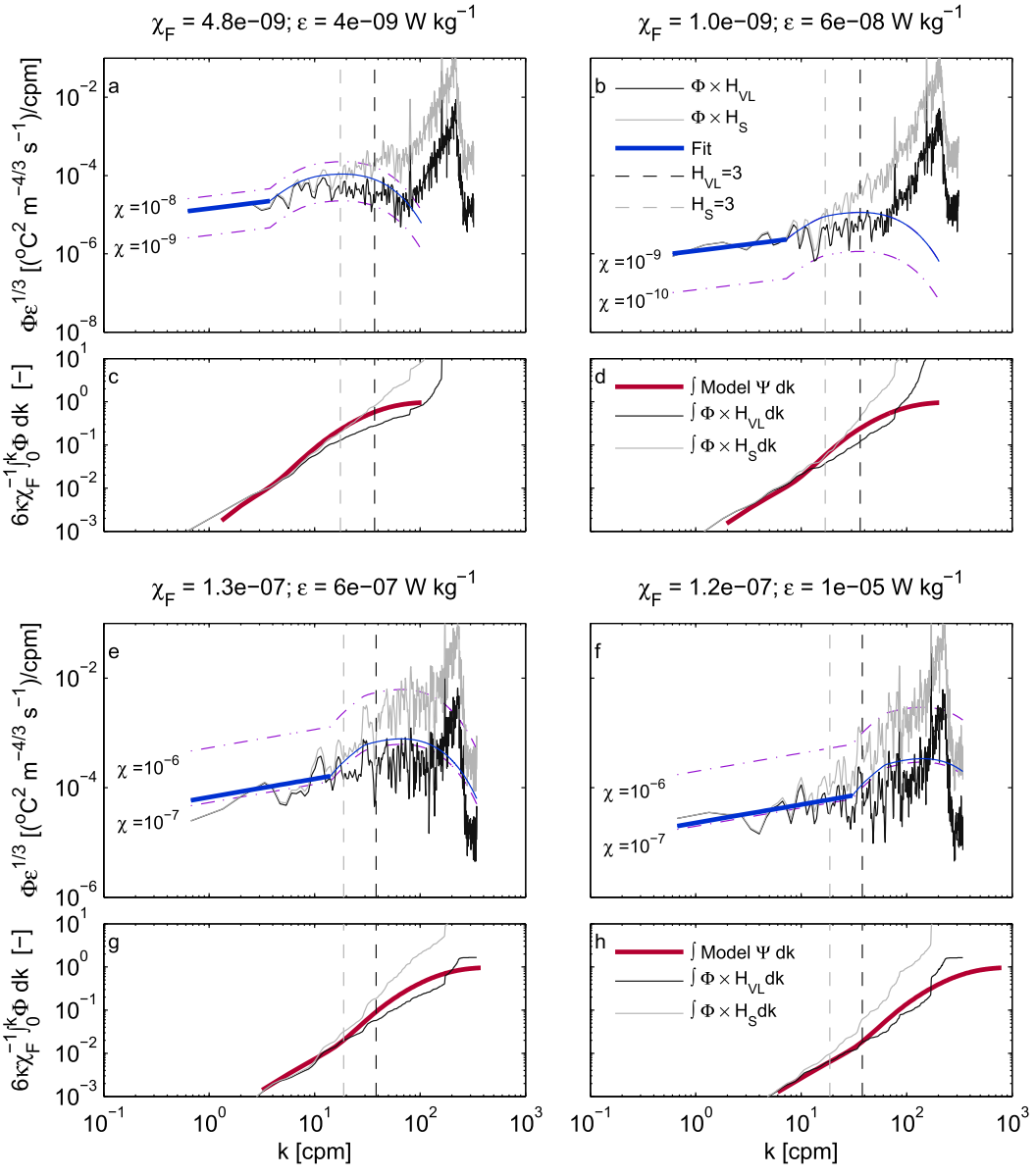


FIG. 2. (a),(b),(e),(f) Examples of $\partial T/\partial x_3$ spectra with increasing $\epsilon$. These examples cover a range of four orders of magnitude of $\epsilon$ with variable $\chi$ where all observed spectra $\Phi$ have been corrected for the thermistor frequency response using $H_{\mathrm{VL}}$ and the more aggressive definition of Sommer et al. (2013) $H_S$. (c),(d),(g),(h) Cumulative integrated spectra for the model and the observed spectra, both are nondimensionalized by $\chi_F$. The effects of applying different thermistor frequency correction factors are also illustrated. Shown are the Kraichnan spectrum for $\chi$ rounded to the nearest order of magnitude above and below $\chi_F$ (violet dotted–dashed lines), and $k_{mI}$ used to obtain $\chi_I$ and generally corresponds to the $k$, where $H = 3$. All model spectrum were estimated from $\chi_F$.

Both methods can be used over the narrow range of conditions when $\mathrm{Re}_b \gtrsim 450$ and $\epsilon \lesssim 5 \times 10^{-8}$ W kg$^{-1}$. For those segments, we compared $\chi_F$ to $\chi_I$ with the two different frequency response corrections (Fig. 3). The $\chi_I$ estimates obtained from the more aggressively corrected spectral observations were in better agreement with $\chi_F$ (violet points in Fig. 3) than $\chi_I$ obtained by applying the weaker frequency correction $H_{\mathrm{VL}}$ (green points in Fig. 3). Nonetheless, the $H_{\mathrm{VL}}$ correction factor still yielded $\chi_I$ that were within a factor of 2 of $\chi_F$, except for very low $\chi_F$ ($\lesssim 3 \times 10^{-9}$°C$^2$s$^{-1}$) when $\chi_I$ exceeded $\chi_F$ or very high $\chi_F$ ($\gtrsim 2 \times 10^{-7}$°C$^2$s$^{-1}$) when $\chi_F$ exceeded $\chi_I$. This factor was less than the error bound associated with $\chi_I$

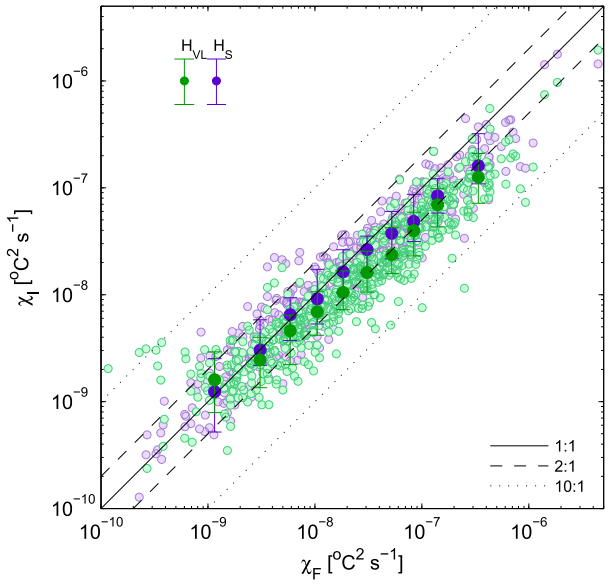


FIG. 3. Scatter of $\chi_I$, obtained by integrating the resolved temperature spectrum, plotted against $\chi_F$, derived by fitting the inertial-convective subrange. Shown are the 571 segments that yielded a reliable estimate for both $\chi_F$ and $\chi_I$. Two separate frequency response corrections were applied to the observed spectral observations, which influence the magnitude of $\chi_I$. Shown are the estimated $\chi_I$ when $H_{VL}$ is applied to the spectra (green) and the $\chi_I$ estimated after applying $H_s$ (purple). The binned data are shown (dark filled markers). The error bars are centered around the median of each bin; the bounds contain 68% of the data (16th and 84th percentiles). Note that integrating our temperature gradient spectra, which have a statistical accuracy of 21 degrees of freedom, yields an error bound for $\chi_I$ of approximately a factor of 2.

obtained by integrating the temperature gradient spectra with 21 degrees of freedom.

From the 4800 segments that yielded a valid estimate for $\epsilon$, more than 4000 segments (83%) returned valid $\chi$ by combining both the integration and fitting techniques. Of the 4800 segments, 2200 (45%) segments returned a valid $\chi_F$ estimate, while 2400 valid $\chi_I$ estimates were obtained during less energetic periods when $\mathrm{Re}_b < 450$. Combining the results from both techniques thus allows us to resolve a very broad range of $\chi$ and hence mixing rates $K_T$ for the 24-h sampling period at this energetic site on the Australian North West shelf (Figs. 4a,b).

The combined dataset shows $\chi$ varied between $10^{-9}$ and $10^{-5}$°C$^2$ s$^{-1}$. The median $\chi_I$ was more than 5 times smaller than the median $\chi_F$, reflecting the fact that the integration method is applicable only during periods of weak $\epsilon$ (Fig. 4a). The mixing rates determined using the Osborn–Cox model [(2)] with just the $\chi_I$ estimates yielded a median $K_T \approx 2 \times 10^{-5}$ m$^2$ s$^{-1}$. The mixing rates obtained with just the $\chi_F$ estimates yielded a median $K_T \approx 8 \times 10^{-4}$ m$^2$ s$^{-1}$ (Fig. 4b)—almost 50 times bigger than those obtained from $\chi_I$. Combining the $K_T$ from both methods results in a (true) median $K_T \approx 1 \times 10^{-4}$ m$^2$ s$^{-1}$, about 5 times higher than the median obtained from just the (traditional) $\chi_I$ estimates.

The estimated $\mathrm{Ri}_f$ [(3)] varied over almost two orders of magnitude with a median $\mathrm{Ri}_f$ not significantly different from the canonical value of 0.17 (Fig. 4c). The median $\mathrm{Ri}_f$ obtained from either technique did not differ significantly from this value, although the median $\mathrm{Ri}_f$ obtained from the fitted $\chi_F$ estimates were slightly larger the median $\mathrm{Ri}_f$ obtained from the integrated $\chi_I$ estimates (Fig. 4c). More dramatic than the median $\mathrm{Ri}_f$ values were the differences in their respective probability distributions. The fitted $\chi_F$ estimates yielded a more skewed distribution with an elongated tail at the low $\mathrm{Ri}_f$ than the distribution of the $\mathrm{Ri}_f$ estimated solely from $\chi_I$. Hence, our spectral-fitting resolves lower $\mathrm{Ri}_f$ that are likely associated with more energetic turbulence periods, that is, high $\mathrm{Re}_b$.

## 5. Conclusions

Without prescribing a value for $\mathrm{Ri}_f$, we have demonstrated a technique that can quantify mixing even in very energetic flows. Our method relies on measuring turbulent temperature fluctuations concurrently with velocity or velocity gradient fluctuations. Once $\epsilon$ is known from the velocity measurements, $\chi$ is obtained by either integrating the viscous-diffusive subrange [(5)] or by fitting the inertial-convective subrange of the temperature gradient spectra [(6)], thus allowing mixing rates to be obtained via the Osborn–Cox model [(2)]. Determining $K_T$ using the inertial-convective subrange is particularly useful in energetic environments because the separation of the largest from the smallest turbulent length scales increases with increasing $\mathrm{Re}_b$. Traditional techniques, such as integrating the viscous-diffusive subrange, are limited to low-energy environments with weak $\epsilon$ (see Fig. 1), and so any temporal or spatial averages of $K_T$ would be biased low unless the spectra were fitted over the inertial-convective subrange. Nevertheless, estimates obtained via integration from low-energy environments can be combined with estimates from fitting in energetic environments to give a comprehensive picture over a wide range of environmental conditions. In addition to the ship-based vertical turbulence profilers considered here, our methods can be applied to moored, horizontally towed, or autonomous profiling instruments. Since most instruments that measure $\epsilon$ also carry the fast-response thermistors necessary to measure $\chi$, our methods can be applied immediately to

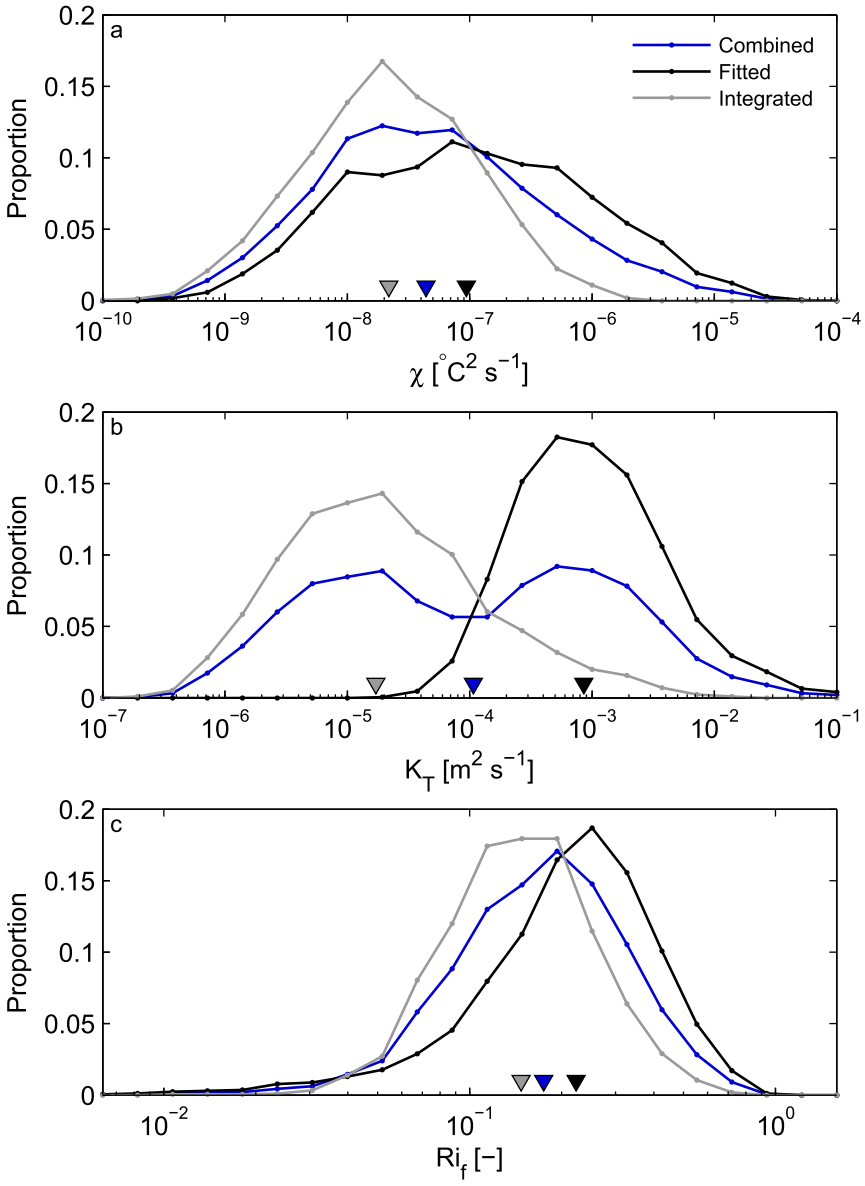


FIG. 4. Line-plot histogram of the estimated (a) $\chi$; (b) $K_T$ from (2), and (c) $\mathrm{Ri}_f = 0.17$ from (3). The combined $\chi$ uses $\chi_I$ when the viscous-diffusive range of $\Phi_{\partial T/\partial x_3}$ are sufficiently resolved, otherwise $\chi_F$ was used, provided $\mathrm{Re}_b \gtrsim 450$. The combined, fitted, and integrated $\chi$ estimates are composed of 4000, 2200, and 2400 samples, respectively. There were almost 600 segments that yielded both integrated and fitted $\chi$ estimates. Excluded from (b) and (c) are the results for which the temperature difference over the vertical extent of the segment was less than twice the accuracy of the thermistor, i.e., $<2 \times 10^{-3}$ °C. Each panel shows the median values (triangles).

existing field datasets to better understand mixing processes in our oceans.

*Acknowledgments.* Funding was provided by the Australian Research Council Discovery Projects (DP 140101322), the Australian Research Council Linkage Project (LP110100017), and the Office of Naval Research (ONR) Naval International Cooperative Opportunities (N62909-11-1-7058). ONR projects ''AUV Data Analysis for Predictability in Time-Evolving Regimes'' and ''Propagation and Dissipation of Internal Tides on Coastal Shelves'' contributed funding for this work. This work was also facilitated by an Institute of Advanced Studies Distinguished Visiting Fellowship

awarded by the University of Western Australia. We thank staff from the Australian Institute of Marine Science, the U.S. Naval Research Laboratory and the University of Western Australia, and the crew of the R/V *Solander*, who aided in the collection of the data.

## REFERENCES


Batchelor, G., 1959: Small-scale variations of convected quantities like temperature in turbulent fluid. *J. Fluid Mech.*, **5**, 113–133, doi:10.1017/S002211205900009X.

Bluteau, C. E., N. L. Jones, and G. N. Ivey, 2011a: Dynamics of a tidally-forced stratified shear flow on the continental slope. *J. Geophys. Res.*, **116**, C11017, doi:10.1029/2011JC007214.

——, ——, and ——, 2011b: Estimating turbulent kinetic energy dissipation using the inertial subrange method in environmental flows. *Limnol. Oceanogr.: Methods*, **9**, 302–321, doi:10.4319/lom.2011.9.302.

——, ——, and ——, 2013: Turbulent mixing efficiency at an energetic ocean site. *J. Geophys. Res. Oceans*, **118**, 4662–4672, doi:10.1002/jgrc.20292.

——, ——, and ——, 2016: Estimating turbulent dissipation from microstructure shear measurements using maximum likelihood spectral fitting over the inertial and viscous subranges. *J. Atmos. Oceanic Technol.*, **33**, 713–722, doi:10.1175/JTECH-D-15-0218.1.

Bogucki, D. J., H. Luo, and J. A. Domaradzki, 2012: Experimental evidence of the Kraichnan scalar spectrum at high Reynolds numbers. *J. Phys. Oceanogr.*, **42**, 1717–1728, doi:10.1175/JPO-D-11-0214.1.

Davis, K. A., and S. G. Monismith, 2011: The modification of bottom boundary layer turbulence and mixing by internal waves shoaling on a barrier reef. *J. Phys. Oceanogr.*, **41**, 2223–2241, doi:10.1175/2011JPO4344.1.

De Lavergne, C., G. Madec, J. L. Sommer, A. J. G. Nurser, and A. C. N. Garabato, 2016: The impact of a variable mixing efficiency on the abyssal overturning. *J. Phys. Oceanogr.*, **46**, 663–681, doi:10.1175/JPO-D-14-0259.1.

Dunckley, J. F., J. R. Koseff, J. V. Steinbuck, S. G. Monismith, and A. Genin, 2012: Comparison of mixing efficiency and vertical diffusivity models from temperature microstructure. *J. Geophys. Res.*, **117**, C10008, doi:10.1029/2012JC007967.

Emery, W. J., and R. E. Thomson, 2001: Data Analysis Methods in Physical Oceanography. 2nd ed. Elsevier Science, 638 pp.

Gargett, A. E., 1997: "Theories" and techniques for observing turbulence in the ocean euphotic zone. *Sci. Mar.*, **61** (Suppl.), 25–45.

——, T. R. Osborn, and P. W. Nasmyth, 1984: Local isotropy and the decay of turbulence in a stratified fluid. *J. Fluid Mech.*, **144**, 231–280, doi:10.1017/S0022112084001592.

Geyer, W. R., M. E. Scully, and D. K. Ralston, 2008: Quantifying vertical mixing in estuaries. *Environ. Fluid Mech.*, **8**, 495–509, doi:10.1007/s10652-008-9107-2.

Goodman, L., E. R. Levine, and R. G. Lueck, 2006: On measuring the terms of the turbulent kinetic energy budget from an AUV. *J. Atmos. Oceanic Technol.*, **23**, 977–990, doi:10.1175/JTECH1889.1.

Goto, Y., I. Yasuda, and M. Nagasawa, 2016: Turbulence estimation using fast-response thermistors attached to a free-fall vertical microstructure profiler. *J. Atmos. Oceanic Technol.*, **33**, 2065–2078, doi:10.1175/JTECH-D-15-0220.1.

Hill, K. D., 1987: Observations of the velocity scaling of thermistor dynamic response functions. *Rev. Sci. Instrum.*, **58**, 1235–1238, doi:10.1063/1.1139444.

Holleman, R. C., W. R. Geyer, and D. K. Ralston, 2016: Stratified turbulence and mixing efficiency in a salt wedge estuary. *J. Phys. Oceanogr.*, **46**, 1769–1783, doi:10.1175/JPO-D-15-0193.1.

Holloway, P. E., P. G. Chatwin, and P. Craig, 2001: Internal tide observations from the Australian North West Shelf in summer 1995. *J. Phys. Oceanogr.*, **31**, 1182–1199, doi:10.1175/1520-0485(2001)031<1182:ITOFTA>2.0.CO;2.

Ivey, G. N., and R. I. Nokes, 1989: Vertical mixing due to the breaking of critical internal waves on sloping boundaries. *J. Fluid Mech.*, **204**, 479–500, doi:10.1017/S0022112089001849.

——, K. B. Winters, and J. R. Koseff, 2008: Density stratification, turbulence, but how much mixing? *Annu. Rev. Fluid Mech.*, **40**, 169–184, doi:10.1146/annurev.fluid.39.050905.110314.

Kraichnan, R. H., 1968: Small-scale structure of a scalar field convected by turbulence. *Phys. Fluids*, **11**, 945–953, doi:10.1063/1.1692063.

Lueck, R. G., F. Wolk, and H. Yamazaki, 2002: Oceanic velocity microstructure measurements in the 20th century. *J. Oceanogr.*, **58**, 153–174, doi:10.1023/A:1015837020019.

Luketina, D., and J. Imberger, 2001: Determining turbulent kinetic energy dissipation from Batchelor curve fitting. *J. Atmos. Oceanic Technol.*, **18**, 100–113, doi:10.1175/1520-0426(2001)018<0100:DTKEDF>2.0.CO;2.

Mater, B. D., and S. K. Venayagamoorthy, 2014: The quest for an unambiguous parameterization of mixing efficiency in stably stratified geophysical flows. *Geophys. Res. Lett.*, **41**, 4646–4653, doi:10.1002/2014GL060571.

Mellor, G. L., and T. Yamada, 1982: Development of a turbulence closure model for geophysical fluid problems. *Rev. Geophys.*, **20**, 851–875, doi:10.1029/RG020i004p00851.

Merrifield, S. T., L. S. Laurent, B. Owens, A. M. Thurnherr, and J. M. Toole, 2016: Enhanced diapycnal diffusivity in intrusive regions of the Drake Passage. *J. Phys. Oceanogr.*, **46**, 1309–1321, doi:10.1175/JPO-D-15-0068.1.

Nash, J. D., D. R. Caldwell, M. J. Zelman, and J. N. Moum, 1999: A thermocouple probe for high-speed temperature measurements in the ocean. *J. Atmos. Oceanic Technol.*, **16**, 1474–1482, doi:10.1175/1520-0426(1999)016<1474:ATPFHS>2.0.CO;2.

Nasmyth, P. W., 1970: Oceanic turbulence. Ph.D. thesis, University of British Columbia, 71 pp., doi:10.14288/1.0302459.

Oakey, N. S., 1982: Determination of the rate of dissipation of turbulent energy from simultaneous temperature and velocity shear microstructure measurements. *J. Phys. Oceanogr.*, **12**, 256–271, doi:10.1175/1520-0485(1982)012<0256:DOTROD>2.0.CO;2.

Osborn, T. R., 1980: Estimates of the local rate of vertical diffusion from dissipation measurements. *J. Phys. Oceanogr.*, **10**, 83–89, doi:10.1175/1520-0485(1980)010<0083:EOTLRO>2.0.CO;2.

——, and C. S. Cox, 1972: Oceanic fine structure. *Geophys. Fluid Dyn.*, **3**, 321–345, doi:10.1080/03091927208236085.

Peltier, W. R., and C. P. Caulfield, 2003: Mixing efficiency in stratified shear flows. *Annu. Rev. Fluid Mech.*, **35**, 135–167, doi:10.1146/annurev.fluid.35.101101.161144.

Rehmann, C. R., and J. R. Koseff, 2004: Mean potential energy change in stratified grid turbulence. *Dyn. Atmos. Oceans*, **37**, 271–294, doi:10.1016/j.dynatmoce.2003.09.001.

Rohr, J. J., E. C. Itsweire, K. N. Helland, and C. W. Van Atta, 1988: Growth and decay of turbulence in a stably stratified shear flow. *J. Fluid Mech.*, **195**, 77–111, doi:10.1017/S0022112088002332.

Ruddick, B., A. Anis, and K. Thompson, 2000: Maximum likelihood spectral fitting: The Batchelor spectrum. *J. Atmos. Oceanic Technol.*, **17**, 1541–1555, doi:10.1175/1520-0426(2000)017<1541:MLSFTB>2.0.CO;2.

Salehipour, H., W. R. Peltier, and A. Mashayek, 2015: Turbulent diapycnal mixing in stratified shear flows: The influence of Prandtl number on mixing efficiency and transition at high Reynolds number. *J. Fluid Mech.*, **773**, 178–223, doi:10.1017/jfm.2015.225.

——, ——, C. B. Whalen, and J. A. MacKinnon, 2016: A new characterization of the turbulent diapycnal diffusivities of mass and momentum in the ocean. *Geophys. Res. Lett.*, **43**, 3370–3379, doi:10.1002/2016GL068184.

Sanchez, X., E. Roget, J. Planella, and F. Forcat, 2011: Small-scale spectrum of a scalar field in water: The Batchelor and Kraichnan models. *J. Phys. Oceanogr.*, **41**, 2155–2167, doi:10.1175/JPO-D-11-025.1.

Sherman, J. T., and R. E. Davis, 1995: Observations of temperature microstructure in NATRE. *J. Phys. Oceanogr.*, **25**, 1913–1929, doi:10.1175/1520-0485(1995)025<1913:OOTMIN>2.0.CO;2.

Shih, L. H., J. R. Koseff, G. N. Ivey, and J. H. Ferziger, 2005: Parameterization of turbulent fluxes and scales using homogeneous sheared stably stratified turbulence simulations. *J. Fluid Mech.*, **525**, 193–214, doi:10.1017/S0022112004002587.

Sommer, T., J. R. Carpenter, M. Schmid, R. G. Lueck, and A. Wuest, 2013: Revisiting microstructure sensor responses with implications for double-diffusive fluxes. *J. Atmos. Oceanic Technol.*, **30**, 1907–1923, doi:10.1175/JTECH-D-12-00272.1.

Sreenivasan, K. R., 1996: The passive scalar spectrum and the Obukhov–Corrsin constant. *Phys. Fluids*, **8**, 189–196, doi:10.1063/1.868826.

Strang, E. J. and H. J. S. Fernando, 2001: Vertical mixing and transports through a stratified shear layer. *J. Phys. Oceanogr.*, **31**, 2026–2048, doi:10.1175/1520-0485(2001)031⟨2026:VMATTA⟩2.0.CO;2.

Tennekes, H., and J. L. Lumley, 1972: *A First Course in Turbulence*. MIT Press, 300 pp.

Vachon, P., and R. Lueck, 1984: A small combined temperature-conductivity probe. *Proc. 1984 STD Conf. and Workshop*, San Diego, CA, Marine Technology Society, 126–131.

Walter, R. K., M. E. Squibb, C. B. Woodson, J. R. Koseff, and S. G. Monismith, 2014: Stratified turbulence in the nearshore coastal ocean: Dynamics and evolution in the presence of internal bores. *J. Geophys. Res. Oceans*, **119**, 8709–8730, doi:10.1002/2014JC010396.

Waterhouse, A. F., and Coauthors, 2014: Global patterns of diapycnal mixing from measurements of the turbulent dissipation rate. *J. Phys. Oceanogr.*, **44**, 1854–1872, doi:10.1175/JPO-D-13-0104.1.

Wolk, F., H. Yamazaki, H. Li, and R. G. Lueck, 2006: Calibrating the spatial response of bio-optical sensors. *J. Atmos. Oceanic Technol.*, **23**, 511–516, doi:10.1175/JTECH1863.1.

Wunsch, C., and R. Ferrari, 2004: Vertical mixing, energy, and the general circulation of the oceans. *Annu. Rev. Fluid Mech.*, **36**, 281–314, doi:10.1146/annurev.fluid.36.050802.122121.